Supplementary Information

Advanced kinetic approach to the multistep thermal dehydration of calcium sulfate dihydrate under different heating and water vapor conditions: kinetic deconvolution and universal isoconversional analyses

Shun Iwasaki, Yuto Zushi, and Nobuyoshi Koga*
Department of Science Education, Division of Educational Sciences, Graduate School of Humanities and Social Sciences, Hiroshima University, 1-1-1 Kagamiyama, Higashi-Hiroshima 739-8524, Japan

Contents

* Corresponding author; e-mail: nkoga@hiroshima-u.ac.jp

S1. Kinetics of the thermal dehydration of CS-DH at different atmospheric $p(H_2O)$ values

S1.1 Mass-loss traces under isothermal conditions

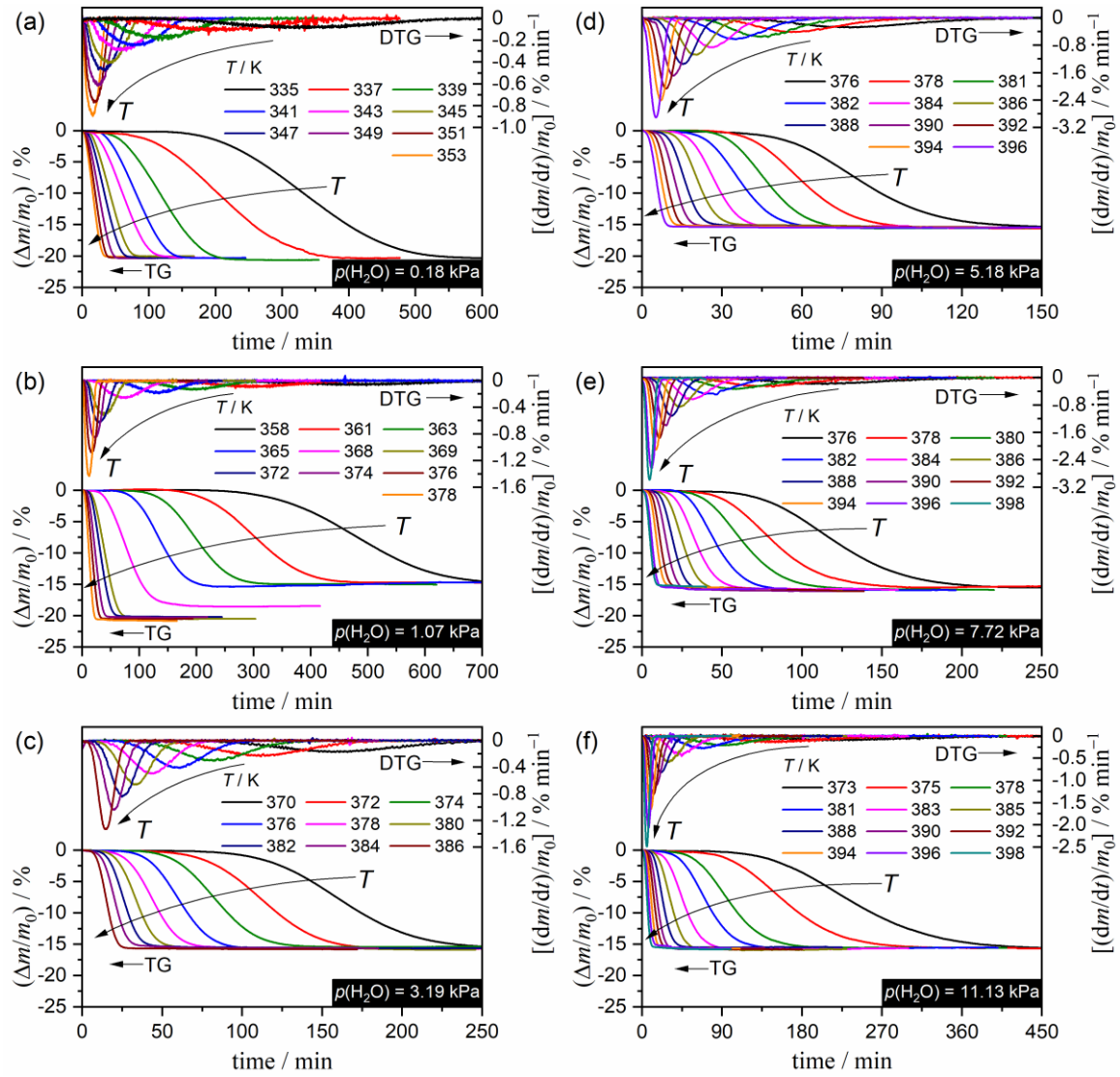

Figure S1. TG–DTG curves recorded under isothermal conditions at different temperatures in a flow of N_2–H_2O mixed gas (q_v = 400 cm^3 min^{-1}) characterized by different $p(H_2O)$ values: (a) $p(H_2O)$ = 0.18 kPa (m_0 = 5.071 ± 0.170 mg), (b) $p(H_2O)$ = 1.07 kPa (m_0 = 5.003 ± 0.026 mg), (c) $p(H_2O)$ = 3.19 kPa (m_0 = 5.032 ± 0.148 mg), (d) $p(H_2O)$ = 5.18 kPa (m_0 = 5.043 ± 0.147 mg), (e) $p(H_2O)$ = 7.72 kPa (m_0 = 4.991 ± 0.093 mg), and (f) $p(H_2O)$ = 11.13 kPa (m_0 = 4.988 ± 0.100 mg).

S1.2 Induction period

Table S1. Arrhenius parameters for the IP processes of the thermal dehydration of CS-DH at each $p(H_2O)$ value, determined by the conventional Arrhenius-type plots without considering the effect of $p(H_2O)$

Subsequent reaction	$p(H_2O)$ / kPa	$E_{a,IP}$ / kJ mol^{-1}	$\ln[A_{IP}f(\alpha_{IP})$ / s$^{-1}]$	$-r$ [a]
CS-DH → Anhydride	0.18	246.3 ± 8.4	76.8 ± 2.9	0.9959
	1.07	355.0 ± 33.4	108.5 ± 10.8	0.9870
CS-DH → CS-HH	1.07	198.4 ± 5.0	57.0 ± 1.7	0.9993
	3.12	213.4 ± 6.3	60.9 ± 2.0	0.9969
	5.16	200.1 ± 10.1	56.1 ± 3.2	0.9937
	7.71	213.6 ± 5.2	60.2 ± 1.7	0.9976
	11.09	213.9 ± 4.7	60.2 ± 1.5	0.9983

[a]Correlation coefficient of the linear regression analysis for the Arrhenius plot.

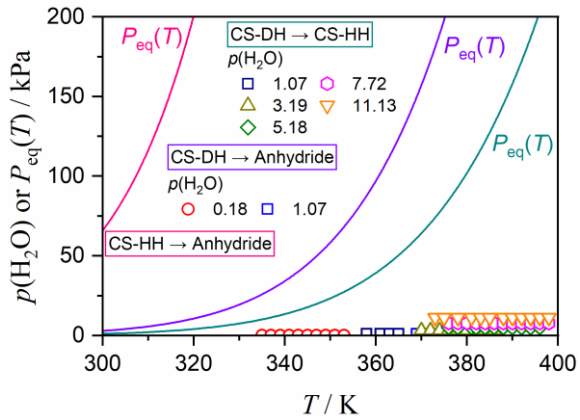

Figure S2. Temperature dependences of $P_{eq}(T)$ for the thermal dehydrations of CS-DH to anhydride, CS-DH to CS-HH, and CS-HH to anhydride, calculated based on a thermodynamic database (MALT-2, Kagaku-Gijutusha), together with the experimentally applied (T, $p(H_2O)$) values.

S1.3 Mass-loss traces under linear nonisothermal conditions

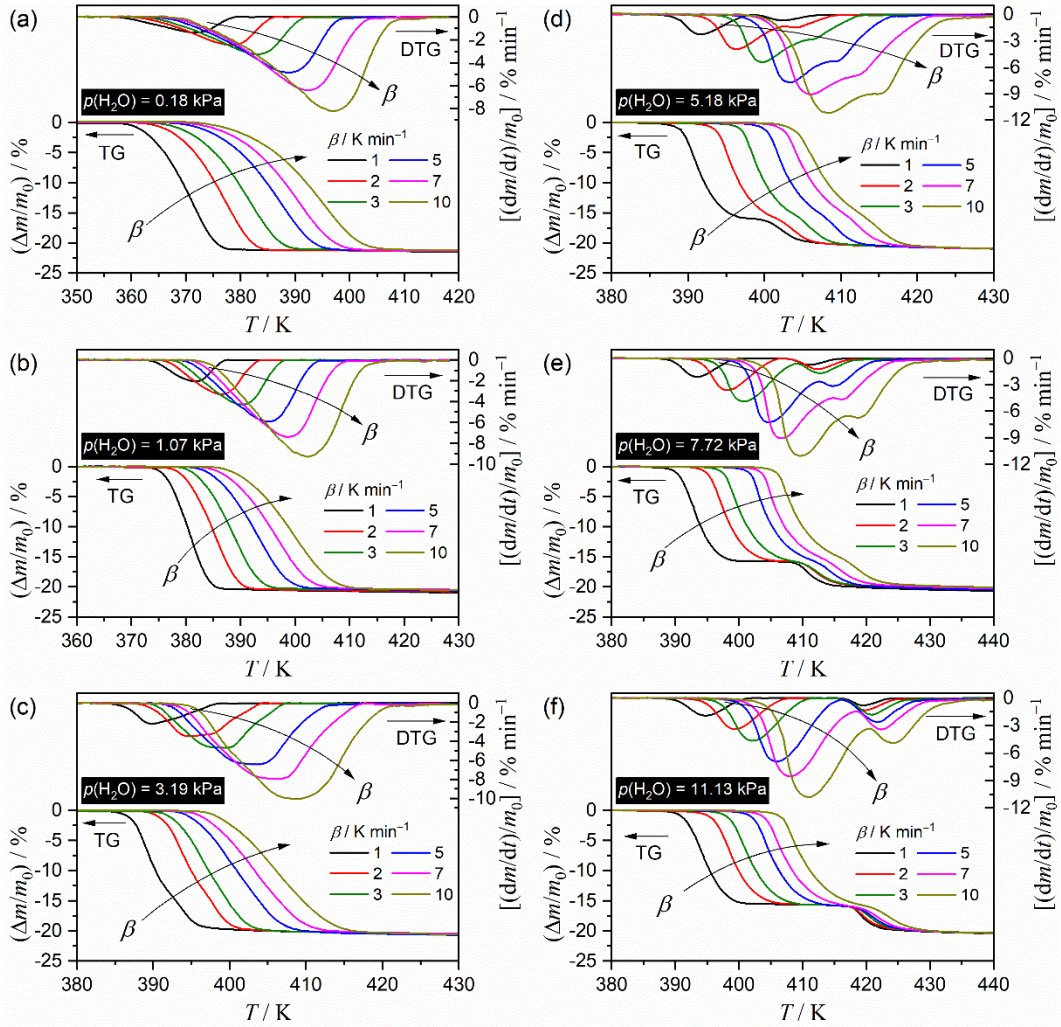

Figure S3. TG–DTG curves for the thermal dehydration of CS-DH recorded under linear nonisothermal conditions at different β values in a flow of the N_2–H_2O mixed gas (q_v = 400 cm^3 min^{-1}) characterized by different $p(H_2O)$ values: (a) $p(H_2O)$ = 0.18 kPa (m_0 = 5.104 ± 0.242 mg), (b) $p(H_2O)$ = 1.07 kPa (m_0 = 5.004 ± 0.032 mg), (c) $p(H_2O)$ = 3.19 kPa (m_0 = 5.045 ± 0.162 mg), (d) $p(H_2O)$ = 5.18 kPa (m_0 = 4.807 ± 0.135 mg), (e) $p(H_2O)$ = 7.72 kPa (m_0 = 5.007 ± 0.024 mg), and (f) $p(H_2O)$ = 11.13 kPa (m_0 = 4.953 ± 0.074 mg).

S1.4 Mathematical deconvolution analysis

MDA was performed for the partially overlapping two-step thermal dehydration process observed under linear nonisothermal conditions at $p(H_2O)$ = 3.19, 5.18, 7.72, and 11.13 kPa. The Weibull function (eq. (S1)) was selected as an appropriate statistical function.

$$F(t) = a_0 \left(\frac{a_3 - 1}{a_3}\right)^{\frac{1-a_3}{a_3}} \left\{\frac{t - a_1}{a_2} + \left(\frac{a_3 - 1}{a_3}\right)^{\frac{1}{a_3}}\right\}^{a_3 - 1} \times \exp\left[-\left\{\frac{t - a_1}{a_2} + \left(\frac{a_3 - 1}{a_3}\right)^{\frac{1}{a_3}}\right\}^{a_3} + \frac{a_3 - 1}{a_3}\right] \quad \text{(S1)}$$

where t is time and a_0–a_3 are the parameters characterizing the amplitude, center, width, and shape, respectively. Figure S4 shows typical MDA results applied to the DTG curves at different $p(H_2O)$ values. The overlapping degree decreases with the increasing $p(H_2O)$ values. The ratio of the separated peak areas for the first and second peaks were estimated to be approximately 3:1, corresponding to the two-step process composed of the thermal dehydration of CS-DH to anhydride via CS-HH. However, an increase in the contribution of the first reaction step was clearly observed with the increasing $p(H_2O)$ value (Table S2).

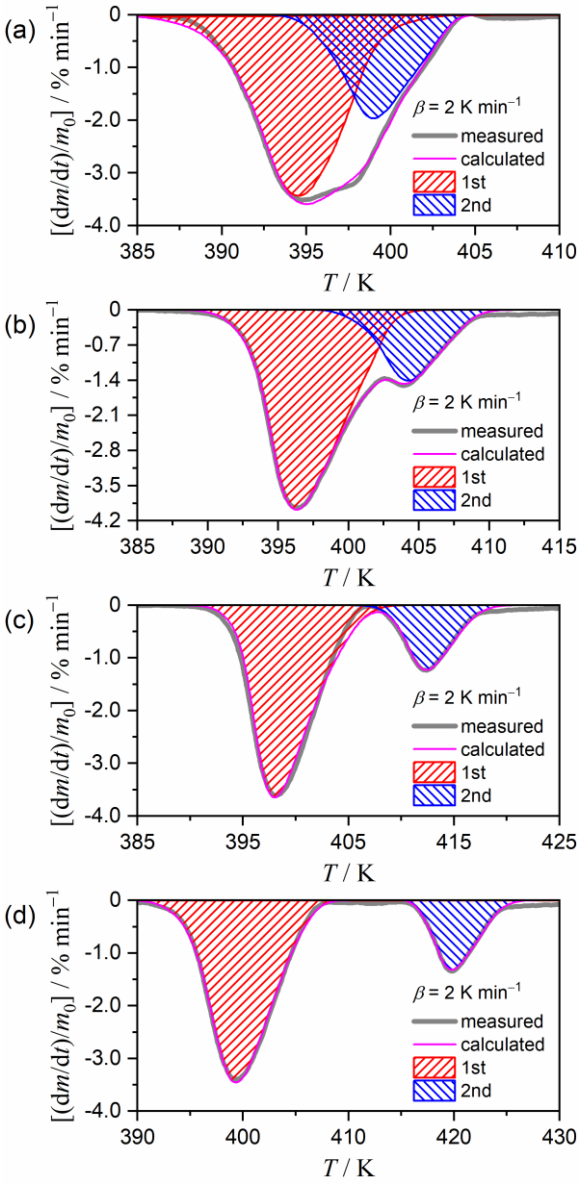

Figure S4. Typical MDA results for the two-step mass-loss process of the thermal dehydration of CS-DH to anhydride via CS-HH at different $p(H_2O)$ values: (a) 3.19, (b) 5.18, (c) 7.72, and (d) 11.13 kPa.

Table S2. The results of MDA and subsequent isoconversional kinetic analysis of the mathematically separated kinetic curves for the thermal dehydrations of CS-DH to CS-HH and CS-HH to anhydride at different $p(H_2O)$ values

i	$p(H_2O)$ / kPa	c_i	$E_{a,i}$ / kJ mol^{-1} [a]	$\frac{d\alpha_i}{d\theta_i} = A_i\alpha_i^{m_i}(1-\alpha_i)^{n_i}[-\ln(1-\alpha_i)]^{p_i}$				
				A_i / s^{-1}	m_i	n_i	p_i	R^2 [b]
1	3.19	0.76 ± 0.02	119.2 ± 1.9	(6.19 ± 0.04) × 10^{13}	−0.18 ± 0.06	1.11 ± 0.02	0.90 ± 0.05	0.9998
	5.18	0.79 ± 0.02	127.8 ± 3.8	(8.43 ± 0.07) × 10^{14}	0.20 ± 0.07	1.11 ± 0.03	0.50 ± 0.07	0.9996
	7.72	0.79 ± 0.02	145.4 ± 4.3	(1.49 ± 0.01) × 10^{17}	0.01 ± 0.07	1.24 ± 0.03	0.70 ± 0.07	0.9998
	11.13	0.80 ± 0.01	143.1 ± 3.4	(5.50 ± 0.03) × 10^{16}	−0.51 ± 0.09	1.38 ± 0.04	1.19 ± 0.09	0.9996
2	3.19	0.24 ± 0.02	137.7 ± 2.7	(2.15 ± 0.01) × 10^{16}	0.17 ± 0.03	1.07 ± 0.01	0.53 ± 0.03	0.9999
	5.18	0.21 ± 0.02	209.2 ± 10.9	(1.51 ± 0.01) × 10^{25}	−0.11 ± 0.06	1.19 ± 0.02	0.69 ± 0.06	0.9997
	7.72	0.21 ± 0.02	351.2 ± 20.7	(4.60 ± 0.06) × 10^{42}	0.06 ± 0.09	1.24 ± 0.03	0.37 ± 0.09	0.9996
	11.13	0.20 ± 0.01	528.2 ± 48.7	(8.12 ± 0.03) × 10^{63}	−1.05 ± 0.07	1.92 ± 0.03	1.43 ± 0.07	0.9999

[a] Averaged over $0.1 \le \alpha_i \le 0.9$.
[b] Determination coefficient of the nonlinear least-squares analysis for fitting the experimental master plot with SB(m_i, n_i, p_i) function.

From the MDA results, a series of kinetic curves at different β values were obtained for each reaction step at different $p(H_2O)$ values as shown in Figures S5–S8. The individual kinetic curve series subjected to an isoconversional kinetic analysis based on eq. (12). Figures S9 and S10 show the Friedman plots at different $p(H_2O)$ values for the first and second reaction steps, respectively. Generally, the Friedman plots exhibited statistically significant linear correlations irrespective of the α_i value. The $E_{a,i}$ values at different α_i values are shown in Figure S11. In each reaction step, the $E_{a,i}$ values increased with the increasing $p(H_2O)$ value. The $E_{a,i}$ values averaged over $0.1 \le \alpha_i \le 0.9$ are also listed in Table S2.

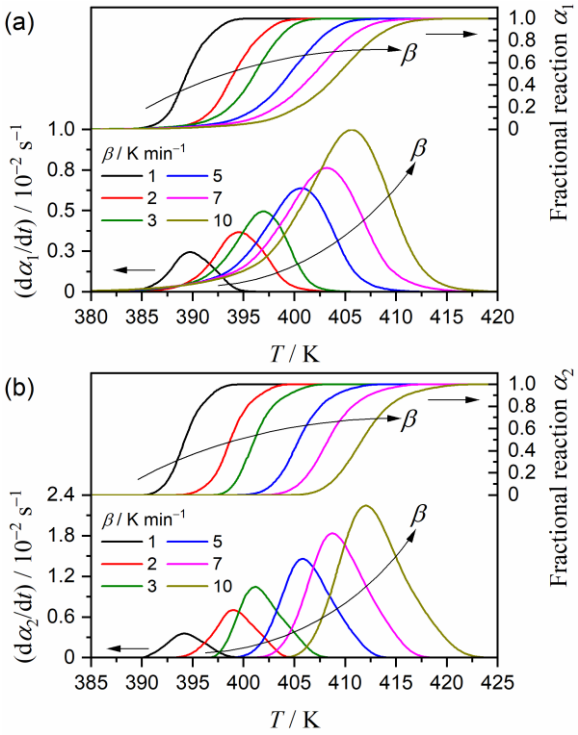

Figure S5. Series of kinetic curves at different β values for each reaction step of the thermal dehydration of CS-DH to anhydride via CS-HH intermediate at $p(H_2O)$ = 3.19 kPa: (a) i = 1 and (b) i = 2.

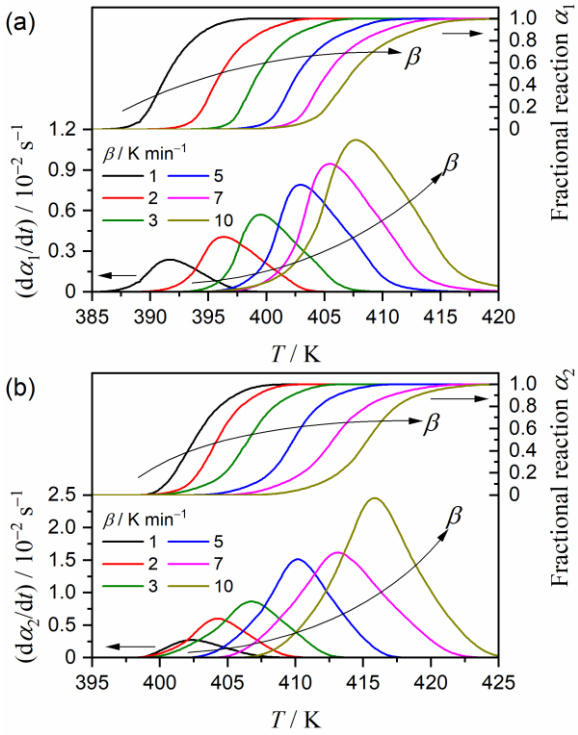

Figure S7. Series of kinetic curves at different β values for each reaction step of the thermal dehydration of CS-DH to anhydride via CS-HH intermediate at $p(H_2O)$ = 7.72 kPa: (a) i = 1 and (b) i = 2.

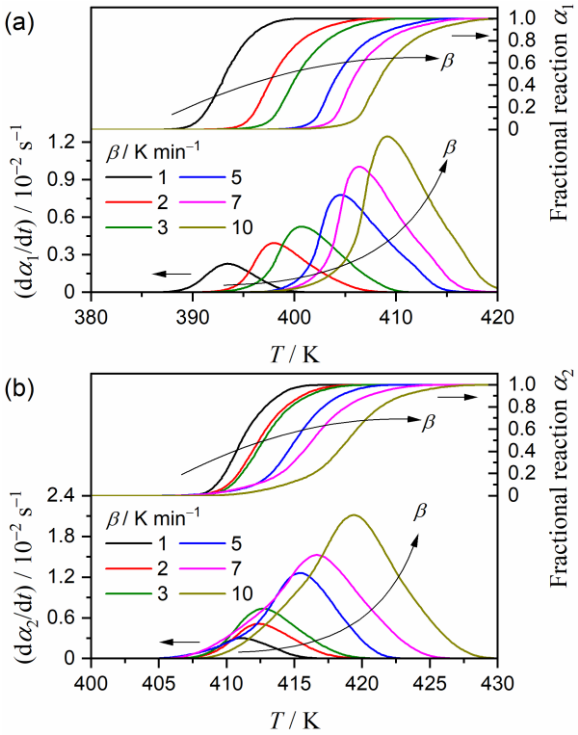

Figure S6. Series of kinetic curves at different β values for each reaction step of the thermal dehydration of CS-DH to anhydride via CS-HH intermediate at $p(H_2O)$ = 5.18 kPa: (a) i = 1 and (b) i = 2.

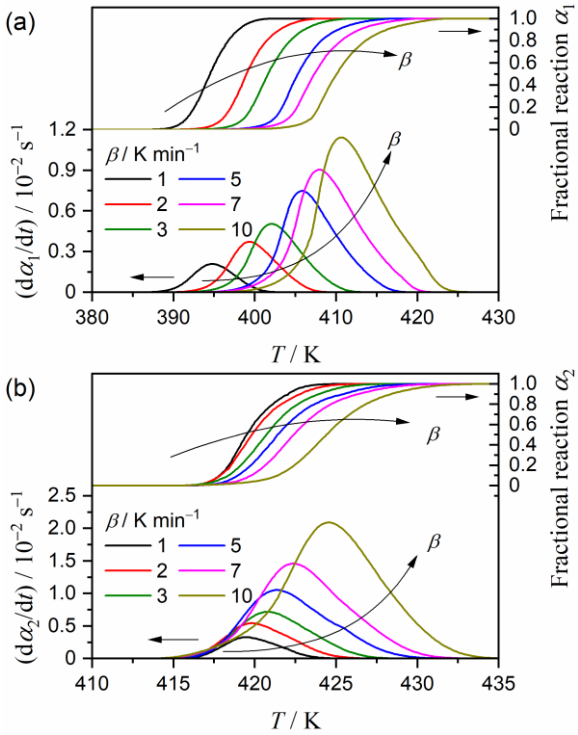

Figure S8. Series of kinetic curves at different β values for each reaction step of the thermal dehydration of CS-DH to anhydride via CS-HH intermediate at $p(H_2O)$ = 11.13 kPa: (a) i = 1 and (b) i = 2.

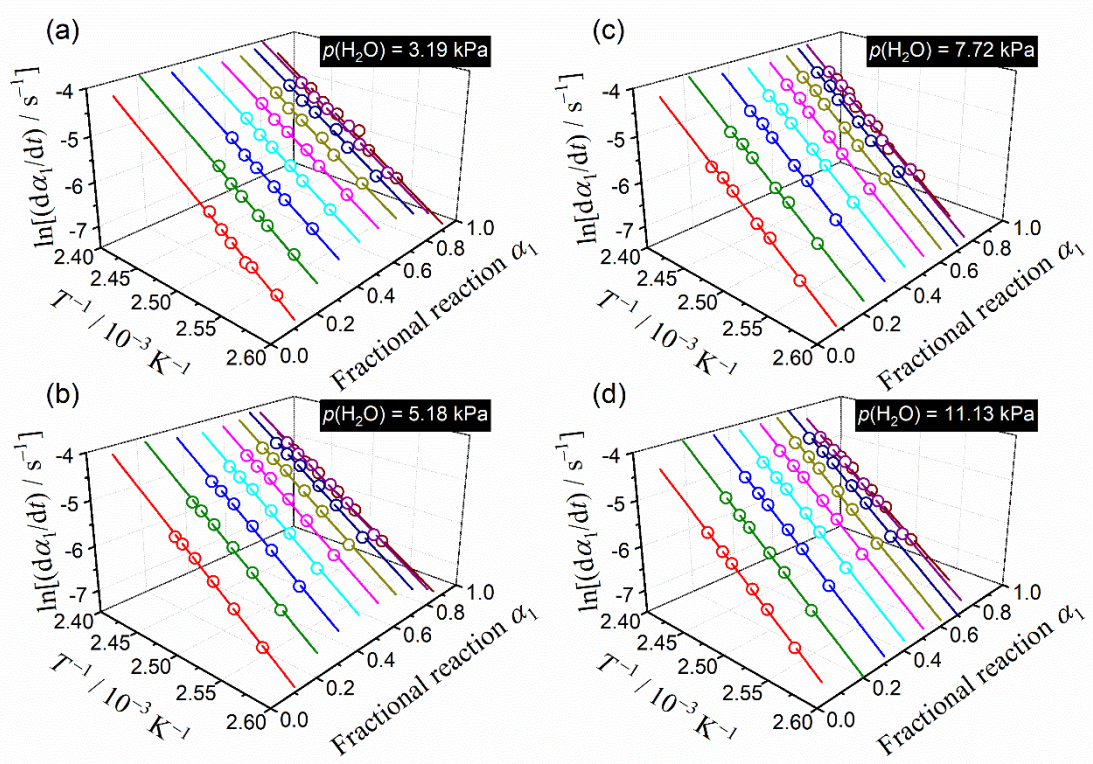

Figure S9. The Friedman plots at different α_1 values for the thermal dehydration of CS-DH to CS-HH intermediate at different $p(H_2O)$ values: (a) 3.19, (b) 5.18, (c) 7.72, and (d) 11.13 kPa.

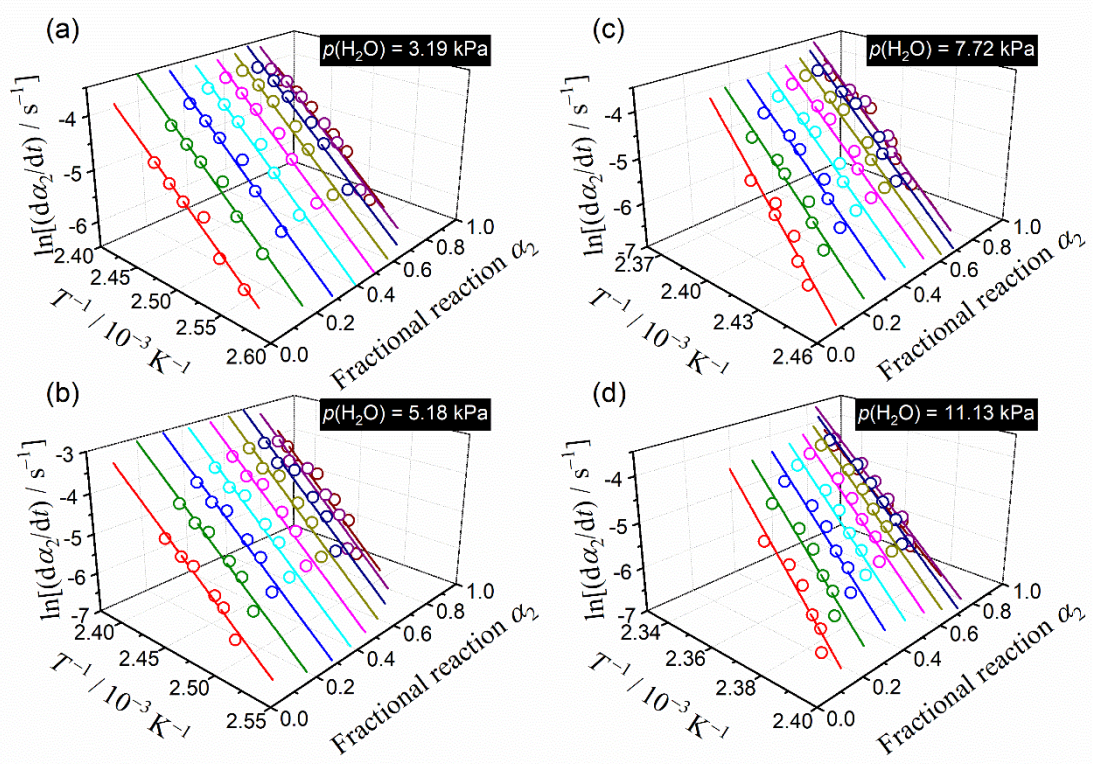

Figure S10. The Friedman plots at different α_2 values for the thermal dehydration of CS-HH intermediate to anhydride at different $p(H_2O)$ values: (a) 3.19, (b) 5.18, (c) 7.72, and (d) 11.13 kPa.

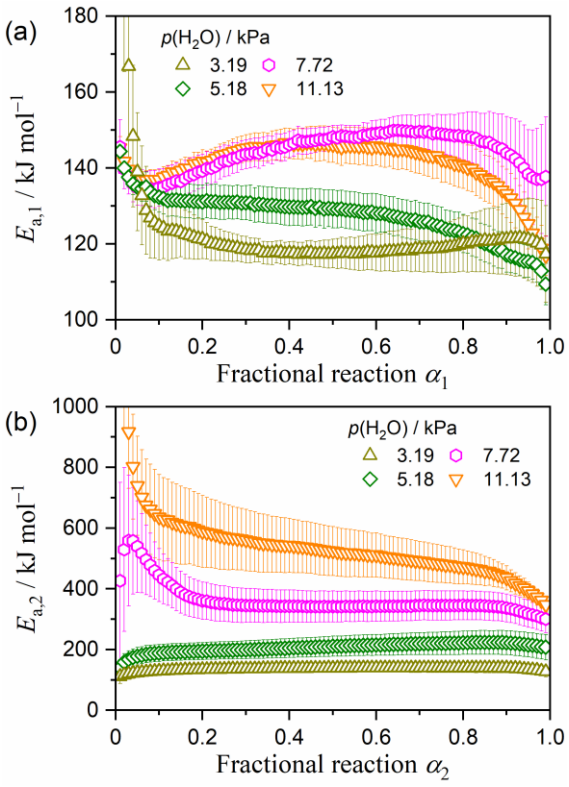

Figure S11. $E_{a,i}$ values at different α_i values for the individual reaction steps of the thermal dehydration of CS-DH at the respective $p(H_2O)$ values: (a) i = 1 and (b) i = 2.

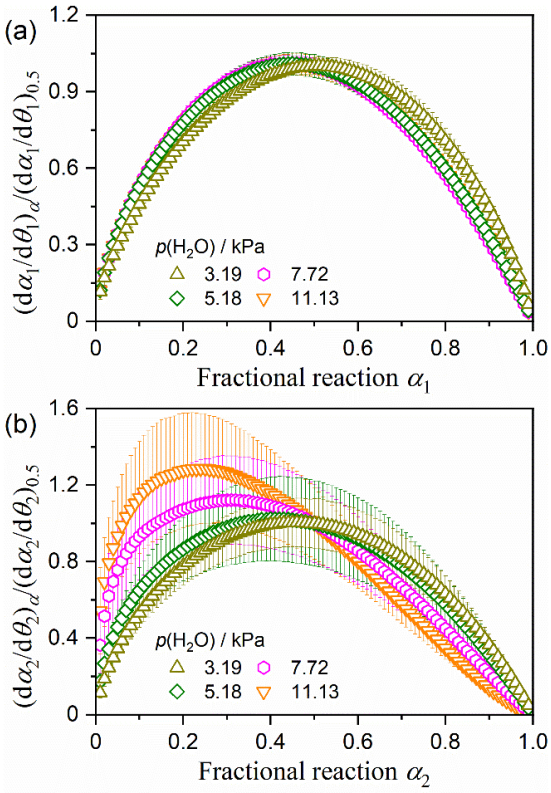

Figure S12. Experimental master plots of $(d\alpha_i/d\theta_i)$ versus α_i normalized by $(d\alpha_i/d\theta_i)$ at α_i = 0.5 at different $p(H_2O)$ values for the individual reaction steps of the thermal dehydration of CS-DH: (a) i = 1 and (b) i = 2.

Figure S12 shows the experimental master plots of $(d\alpha_i/d\theta_i)$ versus α_i normalized by $(d\alpha_i/d\theta_i)$ at α_i = 0.5. Notably, the experimental master plots for the first mass-loss process were invariant irrespective of the $p(H_2O)$ value, wherein the maximum rate was observed midway through the first reaction step. Although the maximum rate appears midway through the second reaction step, the shapes of the experimental master plots vary with the $p(H_2O)$ value accompanied by the systematic shift of the α_i value at the maximum rate to smaller values with the increasing $p(H_2O)$ values. All the experimental master plots were successfully fitted using SB(m_i, n_i, p_i) with the statistically significant correlations ($R^2 > 0.999$). The A_i value and kinetic exponents in SB(m_i, n_i, p_i) obtained by the nonlinear least squares analysis for the fitting are listed in Table S2.

S1.5 Kinetic deconvolution analysis

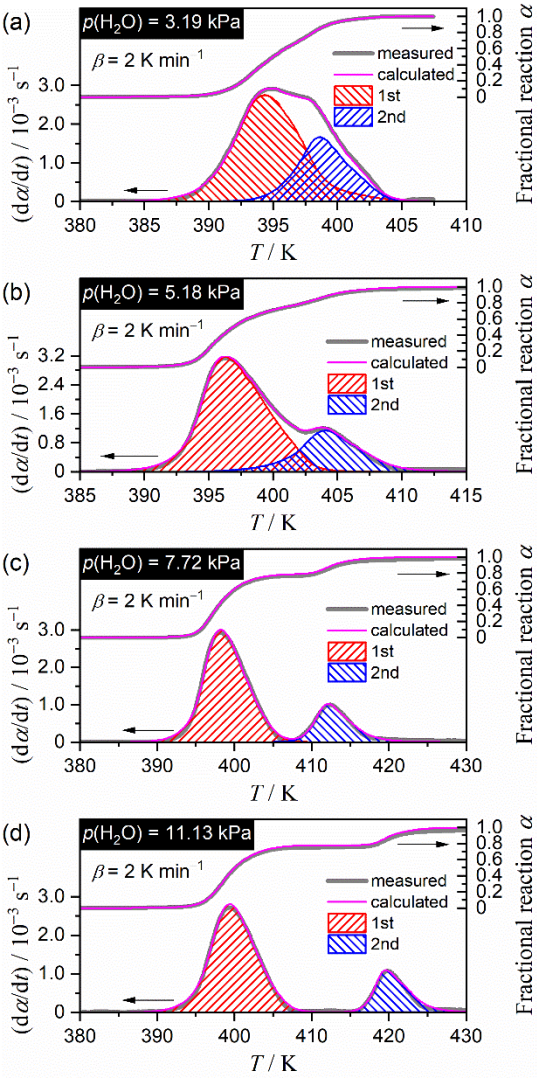

Figure S13. Typical KDA results for the thermal dehydration of CS-DH at different $p(H_2O)$ values: (a) 3.19 kPa, (b) 5.18 kPa, (c) 7.72 kPa, and (d) 11.13 kPa.

Table S3. The kinetic parameters optimized via KDA and averaged over those at different β values for individual reaction steps of the thermal dehydration of CS-DH at different $p(H_2O)$ values

$p(H_2O)$ / kPa	i	c_i	$E_{a,i}$ / kJ mol^{-1}	A_i / s^{-1}	m_i	n_i	p_i	$R^{2,a}$
3.19	1	0.75 ± 0.01	122.5 ± 0.9	(1.82 ± 0.58) × 10^{14}	0.08 ± 0.31	1.09 ± 0.21	0.61 ± 0.35	0.9979 ± 0.0016
	2	0.25 ± 0.01	200.3 ± 0.8	(3.89 ± 1.61) × 10^{24}	0.13 ± 0.08	1.50 ± 0.18	0.72 ± 0.08	
5.18	1	0.78 ± 0.01	126.3 ± 0.9	(6.12 ± 1.51) × 10^{14}	0.43 ± 0.32	1.11 ± 0.15	0.36 ± 0.34	0.9994 ± 0.0002
	2	0.22 ± 0.01	207.7 ± 0.4	(1.44 ± 0.06) × 10^{25}	−0.10 ± 0.01	1.73 ± 0.28	0.93 ± 0.02	
7.72	1	0.80 ± 0.02	144.4 ± 0.5	(1.15 ± 0.18) × 10^{17}	0.01 ± 0.01	1.35 ± 0.07	0.76 ± 0.02	0.9989 ± 0.0002
	2	0.20 ± 0.02	349.3 ± 0.7	(4.33 ± 0.50) × 10^{42}	0.07 ± 0.01	1.94 ± 0.15	0.63 ± 0.04	
11.13	1	0.78 ± 0.01	141.2 ± 1.1	(3.65 ± 0.97) × 10^{16}	0.87 ± 1.03	0.90 ± 0.45	−0.11 ± 1.03	0.9987 ± 0.0001
	2	0.22 ± 0.01	519.1 ± 0.8	(8.26 ± 1.26) × 10^{62}	0.06 ± 0.01	1.95 ± 0.15	0.47 ± 0.13	

[a] Determination coefficient of the nonlinear least-squares analysis of KDA.

S1.6 Isoconversional kinetic analysis for each reaction step at different $p(H_2O)$ values

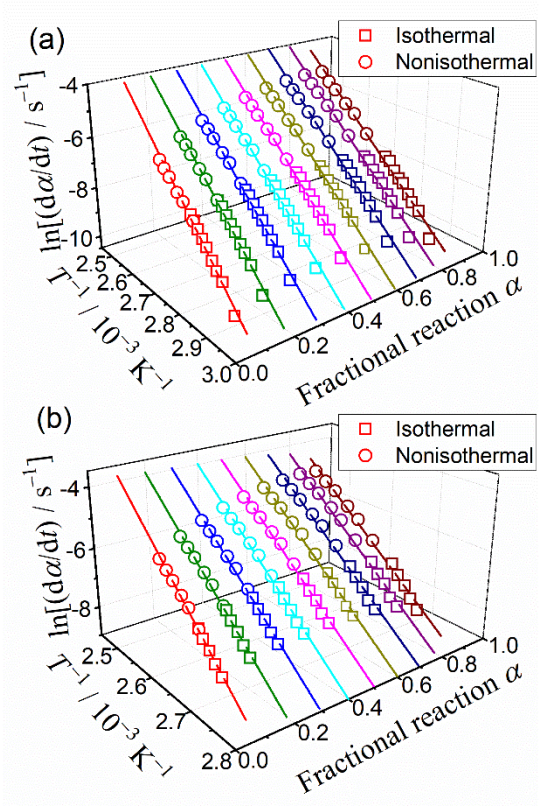

Figure S14. The Friedman plots at various α values for the thermal dehydration of CS-DH to anhydride at different $p(H_2O)$ values: (a) 0.18 and (b) 1.07 kPa.

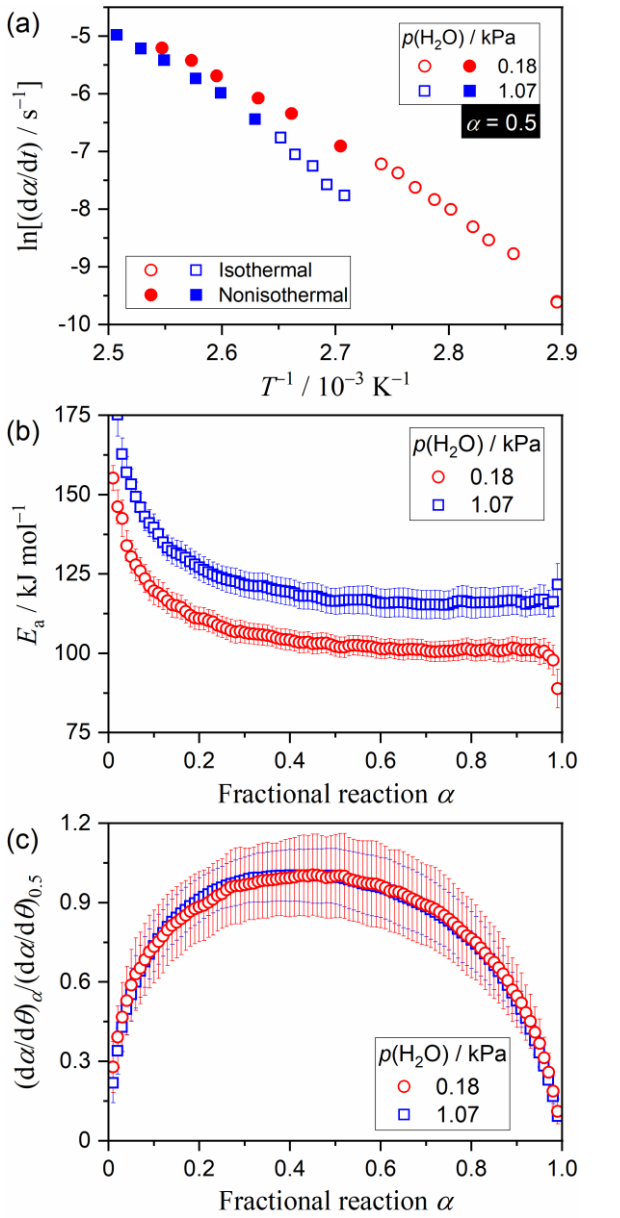

Figure S15. Kinetic results of the conventional isoconversional analysis for the thermal dehydration of CS-DH to anhydride at $p(H_2O)$ of 0.18 and 1.07 kPa: (a) Friedman plots at α = 0.5, (b) E_a values at different α, and (c) experimental master plots of $(d\alpha/d\theta)_\alpha/(d\alpha/d\theta)_{0.5}$ versus α.

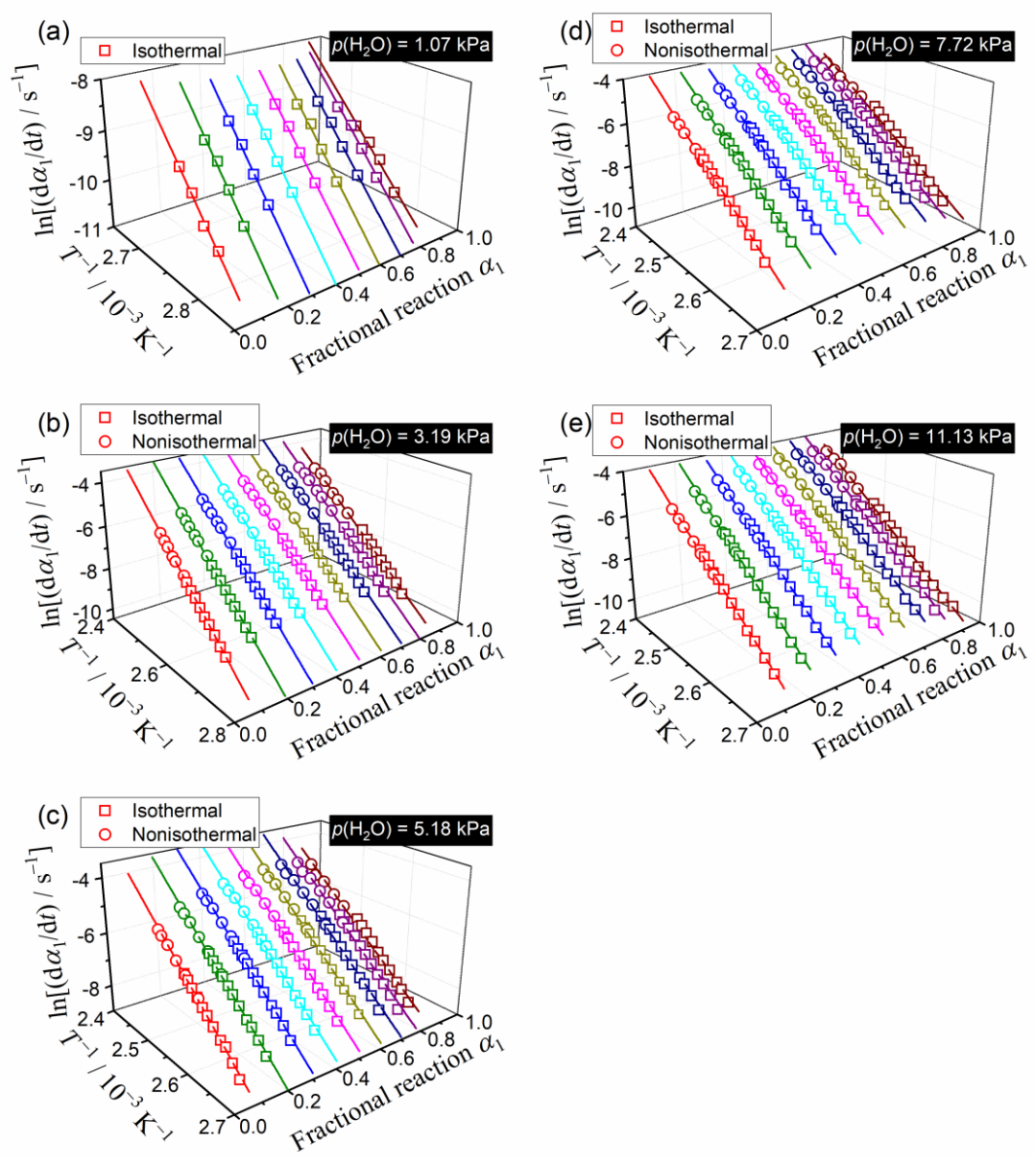

Figure S16. The Friedman plots at various α_1 for the thermal dehydration of CS-DH to CS-HH intermediate at different $p(H_2O)$ values: (a) 1.07, (b) 3.19, (c) 5.18, (d) 7.72 and (e) 11.13 kPa.

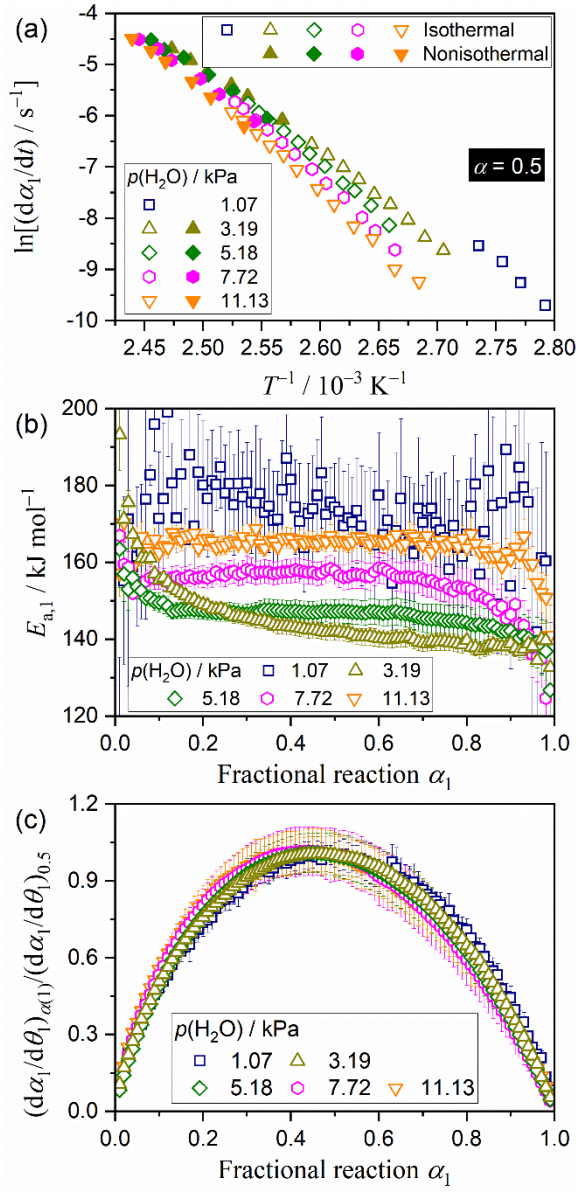

Figure S17. Kinetic results of the conventional isoconversional analysis for the thermal dehydration of CS-DH to CS-HH intermediate at $p(H_2O)$ of 1.07, 3.19, 5.18, 7.72, and 11.13 kPa: (a) Friedman plots at α_1 = 0.5, (b) $E_{a,1}$ values at different α_1 values, and (c) experimental master plots of $(d\alpha_1/d\theta_1)_{\alpha(1)}/(d\alpha_1/d\theta_1)_{0.5}$ versus α_1.

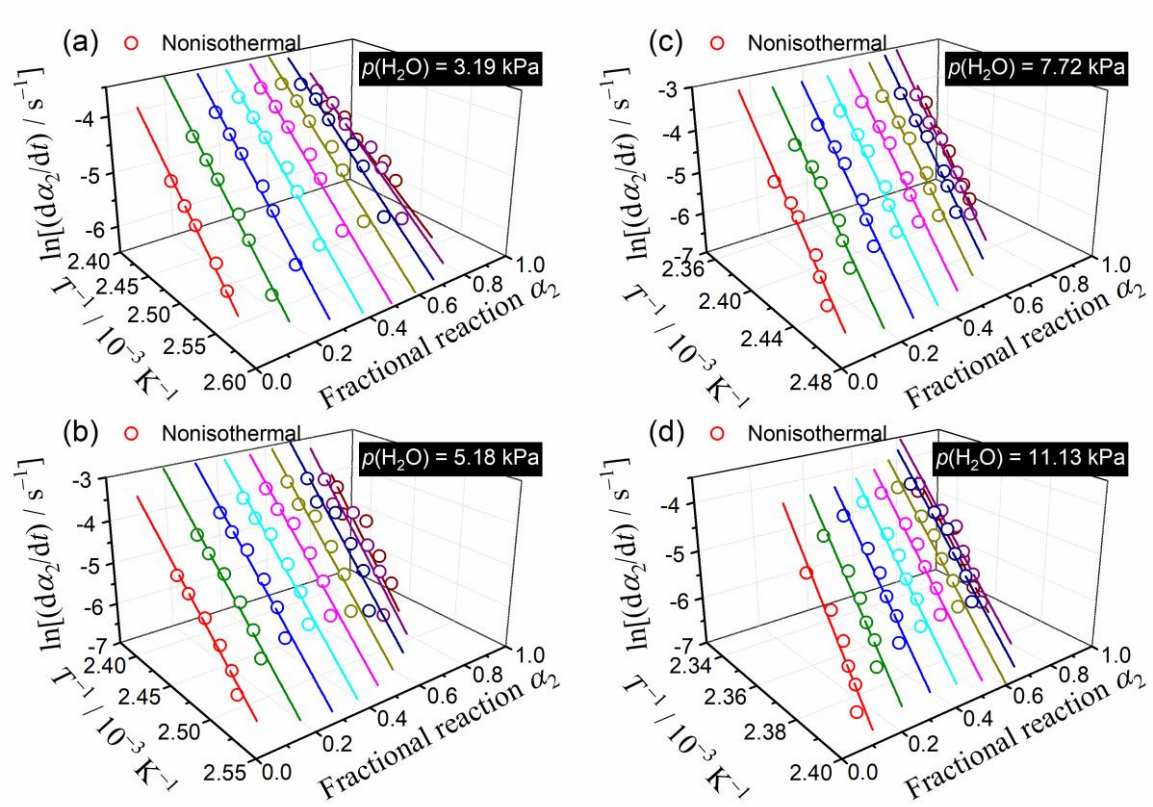

Figure S18. The Friedman plots at various α_2 values for the thermal dehydration of CS-HH intermediate to anhydride at different $p(H_2O)$ values: (a) 3.19, (b) 5.18, (c) 7.72, and (d) 11.13 kPa.

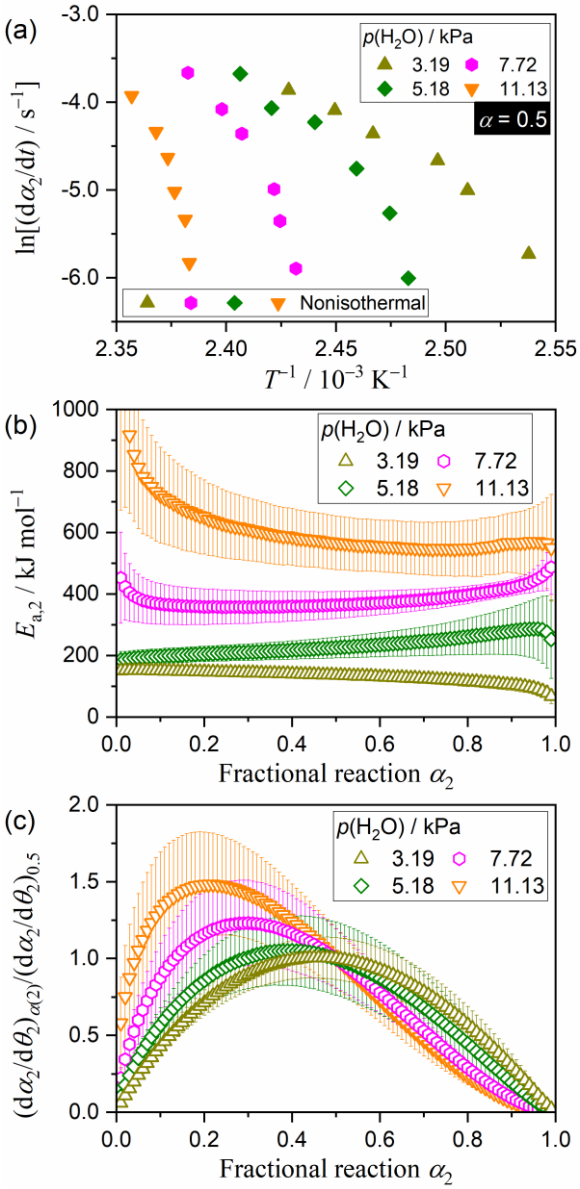

Figure S19. Kinetic results of the conventional isoconversional analysis for the thermal dehydration of CS-HH intermediate to anhydride at $p(H_2O)$ of 3.19, 5.18, 7.72, and 11.13 kPa: (a) Friedman plots at α_2 = 0.5, (b) $E_{a,2}$ values at different α_2 values, and (c) experimental master plots of $(d\alpha_2/d\theta_2)_{\alpha(2)}/(d\alpha_2/d\theta_2)_{0.5}$ versus α_2.

Table S4. The apparent kinetic parameters determined by the conventional isoconversional analysis without considering the effect of $p(H_2O)$ for the thermal dehydration processes of CS-DH to anhydride, CS-DH to CS-HH intermediate, and CS-HH intermediate to anhydride at different $p(H_2O)$ values

Reaction process	$p(H_2O)$ / kPa	$E_{a,i}$ / kJ mol^{-1}, [a]	$\frac{d\alpha_i}{d\theta_i} = A_i\alpha_i^{m_i}(1-\alpha_i)^{n_i}[-\ln(1-\alpha_i)]^{p_i}$				
			A_i / s^{-1}	m_i	n_i	p_i	$R^{2, b}$
CS-DH → anhydride	0.18	104.8 ± 4.9	(1.07 ± 0.01) × 10^{12}	−0.84 ± 0.08	0.97 ± 0.03	1.20 ± 0.08	0.9986
(i = non)	1.07	119.9 ± 5.8	(7.80 ± 0.14) × 10^{13}	−0.78 ± 0.14	1.01 ± 0.05	1.17 ± 0.13	0.9974
CS-DH → CS-HH	1.07	173.1 ± 8.3	(3.14 ± 0.05) × 10^{21}	0.78 ± 0.14	0.77 ± 0.05	−0.05 ± 0.14	0.9985
(i = 1)	3.19	143.1 ± 4.7	(9.34 ± 0.04) × 10^{16}	0.26 ± 0.04	1.03 ± 0.02	0.46 ± 0.03	0.9999
	5.18	146.4 ± 1.6	(2.60 ± 0.02) × 10^{17}	1.12 ± 0.06	0.81 ± 0.02	−0.32 ± 0.06	0.9998
	7.72	155.6 ± 2.8	(3.51 ± 0.04) × 10^{18}	1.35 ± 0.10	0.75 ± 0.04	−0.57 ± 0.10	0.9996
	11.13	165.1 ± 1.7	(4.73 ± 0.04) × 10^{19}	1.41 ± 0.07	0.66 ± 0.03	−0.68 ± 0.07	0.9997
CS-HH → anhydride	3.19	133.4 ± 12.6	(7.43 ± 0.02) × 10^{15}	0.36 ± 0.03	1.30 ± 0.01	0.55 ± 0.03	0.9999
(i =2)	5.18	230.2 ± 22.9	(1.05 ± 0.01) × 10^{28}	0.09 ± 0.03	1.57 ± 0.01	0.71 ± 0.03	0.9999
	7.72	373.2 ± 17.6	(4.54 ± 0.02) × 10^{45}	0.16 ± 0.03	1.91 ± 0.02	0.52 ± 0.03	0.9999
	11.13	588.0 ± 45.9	(2.68 ± 0.01) × 10^{71}	−1.74 ± 0.13	2.71 ± 0.06	2.19 ± 0.13	0.9999

[a] Averaged over $0.1 \leq \alpha_i \leq 0.9$.

[b] Determination coefficient of the nonlinear least-squares analysis for fitting the experimental master plots with SB(m_i, n_i, p_i) function.

S2. Kinetics of the thermal dehydration of the CS-HH reagent at different atmospheric $p(H_2O)$ values

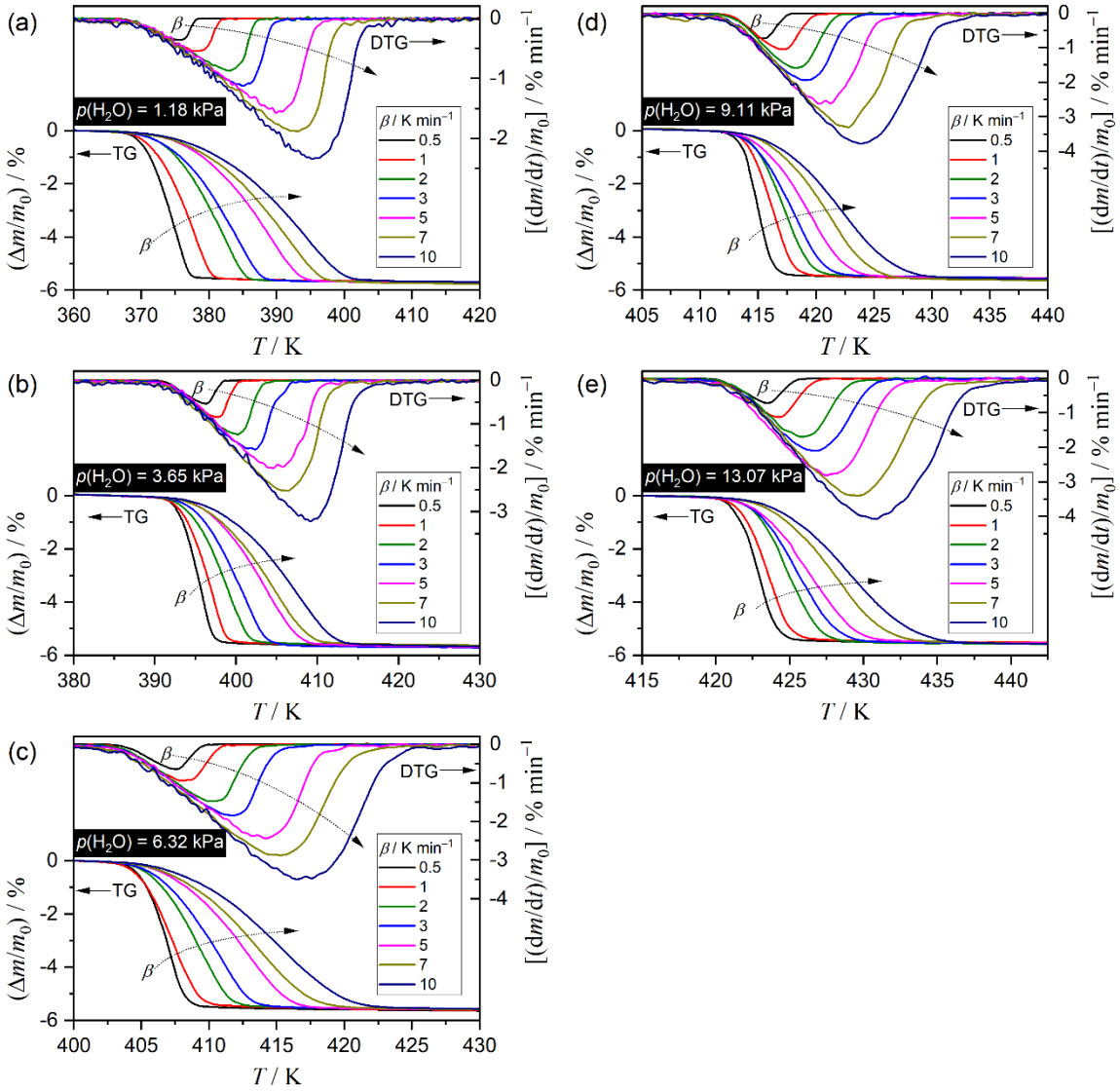

Figure S20. TG–DTG curves for the thermal dehydration of CS-HH reagent under linear nonisothermal conditions at different β values, recorded in flowing N_2–H_2O mixed gas characterized by different $p(H_2O)$ values: (a) $p(H_2O)$ = 1.18 ± 0.03 kPa (m_0 = 9.99 ± 0.03 mg), (b) $p(H_2O)$ = 3.65 ± 0.07 kPa (m_0 = 10.00 ± 0.04 mg), (c) $p(H_2O)$ = 6.32 ± 0.16 kPa (m_0 = 9.98 ± 0.02 mg), (d) $p(H_2O)$ = 9.11 ± 0.18 kPa (m_0 = 9.99 ± 0.04 mg), and (e) $p(H_2O)$ = 13.07 ± 0.11 kPa (m_0 = 10.01 ± 0.04 mg).

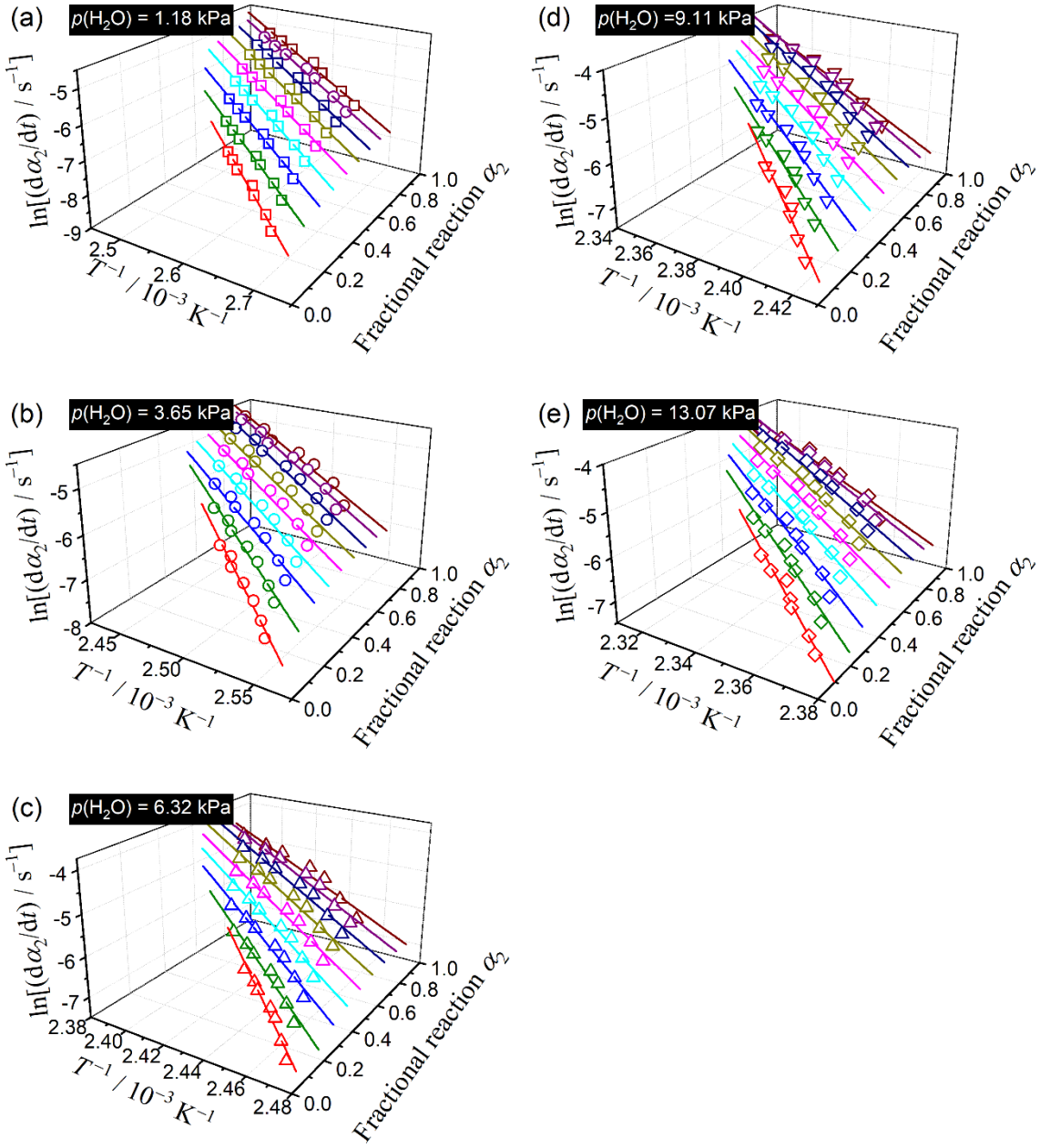

Figure S21. The Friedman plots for the thermal dehydration of the CS-HH reagent at different $p(H_2O)$ values.

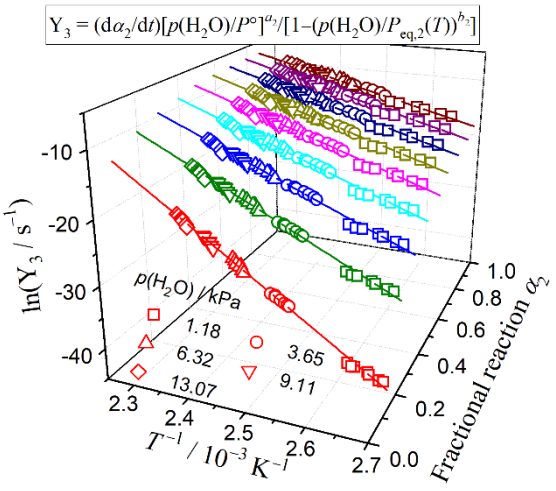

Figure S22. The universal Friedman plots for the thermal dehydration of the CS-HH reagent over different $p(H_2O)$ values.

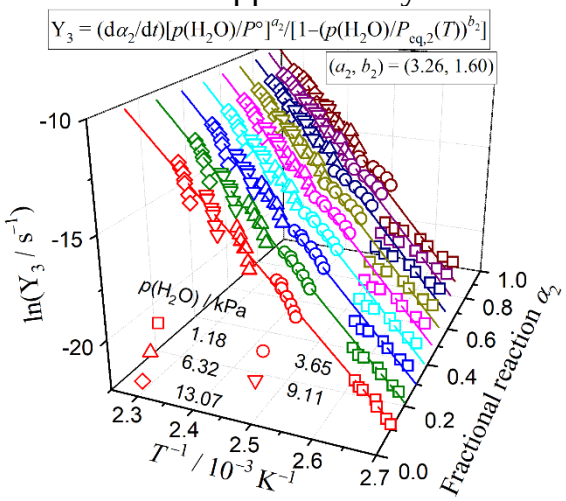

Figure S23. The universal Friedman plots for the thermal dehydration of the CS-HH reagent over different $p(H_2O)$ values, performed by setting the exponents (a_2, b_2) in the AF as the average values (3.26, 1.60).